Environmental Science and Pollution Research (2022) 29:69439–69449
https://doi.org/10.1007/s11356-022-20673-5

RESEARCH ARTICLE

Glutaraldehyde base-cross-linked chitosan-silanol/Fe_3O_4 composite for removal of heavy metals and bacteria

Qibo Liu[1] · Yonghui Wang[2] · Xueli Liu[2] · Shuang Li[2] · shuyue Ren[2] · Zhixian Gao[2] · Tie Han[2] · Zhangrun Xu[1] · Huanying Zhou[2]

Received: 21 December 2021 / Accepted: 3 May 2022 / Published online: 14 May 2022

Abstract

We designed and synthesised a magnetic adsorbent (Fe_3O_4@Si–OH@CS-Glu) combining chitosan-silanol groups with glutaraldehyde as a cross-linking agent, which has improved physicochemical properties and can be used to remove multiple heavy metals and bacteria from polluted water. The adsorbent was characterised with SEM, XRD, FTIR, BET, VSM, and zeta potential. Under optimum conditions, the adsorption efficiencies of Fe_3O_4@Si–OH@CS-Glu for Cr^{6+}, As^{5+}, Hg^{2+}, and Se^{6+} were as high as 90.5%, 73.5%, 91.6%, and 100% respectively. In addition, *Escherichia coli* (gram-negative) and *Staphylococcus aureus* (gram-positive) can be removed after 2–4 adsorption cycles with 2.5 mg Fe_3O_4@Si–OH@CS-Glu. The main adsorption mechanism of the adsorbent for heavy metals and bacteria is electrostatic adsorption. Overall, the synthesised Fe_3O_4@Si–OH@CS-Glu adsorbent showed high removal efficiency and adsorption capacity with a stable structure and easy separation. It has promising applications for the removal of heavy metals and bacteria from water.

Keywords Bacteria · Chitosan · Glutaraldehyde · Heavy metals · Magnetic composite · Silanol groups

Introduction

Water pollution, caused by illegal discharge of wastewater, accidental leakage of raw materials, and poor water management or monitoring, has severely affected water quality and safety (Gothandam et al. 2020). The pollutants can include organic pollutants, heavy metals, pharmaceuticals, and drug-resistant bacteria (Chen and Huang 2020). Among those contaminants, heavy metals are toxic, accumulative, non-degradable, and carcinogenic (Leus et al. 2018). In addition, antibiotics and other chemicals induce drug-resistant bacteria. Therefore, heavy metals and bacteria pose an enormous threat to human health (Hashim et al. 2011; Na et al. 2021). At present, there are various methods for removing heavy metals or bacteria from water. The commonly used methods include adsorption, membrane filtration, wet heat sterilisation, chemical precipitation, and electrochemical treatment (Ince et al. 2020; Bairagi and Ali 2020). The adsorption method has been widely used for the removal of pollutants from water because of its advantages such as low cost, high adsorption efficiency, simple operation, and short adsorption cycle (Liu et al. 2019; Panda et al. 2020).

Chitosan (CS), derived from chitin, is one of the most abundant biopolymers in nature (Gabriel et al. 2020). Chitosan contains many functional groups (amino, acetamido, and hydroxyl groups) that can be used as active sites for pollutant removal. Therefore, chitosan has been widely used in the removal of heavy metals and bacteria (Tanhaei et al. 2015; Altun et al. 2020; Anwar et al. 2020; Sharma et al. 2016; Nayak et al. 2015; Dobrzyńska 2021; Guo et al. 2014; Wu et al. 2017). However, in highly acidic conditions, CS has the disadvantages of a high expansion index, poor mechanical properties, and small specific surface area, which greatly limits its application (Habiba

Responsible Editor: Angeles Blanco

Yonghui Wang contributed equally to this work.

✉ Huanying Zhou
zhouhytj@163.com

[1] Research Center for Analytical Sciences, Northeastern University, Shenyang 110819, China

[2] Tianjin Key Laboratory of Risk Assessment and Control Technology for Environment and Food Safety, Tianjin Institute of Environmental and Operational Medicine, Tianjin 300050, China

et al. 2017; Jawad et al. 2020a). It is therefore necessary to modify chitosan so that its physicochemical properties are improved.

Currently, various methods exist to enhance the physical and chemical properties of chitosan, such as cross-linking reactions (Jiang et al. 2019; Nnam et al. 2021; Reghioua et al. 2021a), complexation with metal oxide nanoparticles (Dehaghi et al. 2014), and the functionalisation of organic groups (Li et al. 2019). The cross-linking method involves combining the target with the functional groups on the cross-linking agent and is a common method for modifying chitosan at present (Zhang et al. 2018; Reghioua et al. 2021b; Ahj et al. 2021). Glutaraldehyde (Glu) is a cross-linking agent with dialdehyde functional groups, which can react with -NH_2 and -OH on the main chain of chitosan to form an ionic cross-linking network, improving the stability and mechanical strength of chitosan (Ahj et al. 2020; Abdulhameed et al. 2019; Reghioua et al. 2021c). However, this cross-linking reaction would block the active sites of CS, leading to a decrease in its adsorption capacity (Mohammad et al. 2019; Malek et al. 2020). Adding nanomaterials with multifunctional clusters into CS molecules can effectively improve the adsorption capacity (Nishad et al. 2017; Jawad et al. 2021).

The surface of SiO_2 contains a large number of -OH functional groups. Cross-linking CS with SiO_2 can effectively improve its adsorption performance and antibacterial properties (Mortazavi et al. 2010; Nawaz et al. 2020; Reis et al. 2002; Allen et al. 2007). Recently, magnetic materials have attracted much attention as adsorbents, as they are easily separated through magnetic solid-phase extraction (MSPE). Fe_3O_4 nanoparticles have attracted extensive attention due to their advantages of stable structure, convenient production, low cost, and easy separation and regeneration (Panda et al. 2020; Wang et al. 2020). However, Fe_3O_4 also has the disadvantage of easy oxidation and agglomeration, which prevent the desired effect from being achieved in many applications. Recently, several researchers have attempted to improve the stability and antioxidant properties of Fe_3O_4 by coating it with SiO_2 and grafting some functional groups. The physical and chemical properties of the modified particles are improved (Koo et al. 2019).

In this work, a glutaraldehyde base-cross-linked chitosan-silanol/Fe_3O_4 composite was synthesised. Combining with MSPE technology, Fe_3O_4@Si–OH@CS-Glu was used as an adsorbent for simultaneous removal of heavy metals and bacteria from water. This adsorbent combines the advantages of the materials described above. It is easy to be separated with a high adsorption performance. We also determined the optimal conditions for the removal of heavy metals and bacteria which included pH, removal time, and adsorbent dosage. The adsorption mechanism was also briefly described.

Materials and methods

Materials

Ferrous sulfate ($FeSO_4{\cdot}7H_2O$), ammonium hydroxide ($NH_3{\cdot}H_2O$, 25–28%), glutaraldehyde ($C_5H_8O_2$, 50% solution), and glacial acetic acid (CH_3COOH) were obtained from Tianjin Fengchuan Chemical Reagent Co., Ltd. Anhydrous ethanol (C_2H_5OH) was obtained from Tianjin Damao Chemical Reagent Factory. Ethyl orthosilicate ($C_8H_{20}O_4Si$, 28%) was obtained from Tianjin Jinke Fine Chemical Research Institute. Chitosan ($C_6H_{12}NO_4$, low viscosity < 200 mPa s), hydrochloric acid (HCl), and ferric chloride hexahydrate ($FeCl_3{\cdot}6H_2O$) were purchased from Tianjin Fuchen Chemical Reagent Factory. All reagents were of analytical grade and were used directly as received without further treatment. Ultrapure water with a resistivity of 18 MΩ/cm was used for all the experiments.

Synthesis of Fe_3O_4@Si–OH@CS-Glu

Fe_3O_4@Si–OH were prepared using a previously reported method (Tang et al. 2019). First, $FeCl_3{\cdot}6H_2O$ (5.21 g) and $FeSO_4{\cdot}7H_2O$ (4.22 g) were added to 250 mL of deionised water. HCl (850 µL) was then added to the mixture and subjected to ultrasonic deoxidisation for 30 min. Then, 22 mL of $NH_3{\cdot}H_2O$ was added to the solution after ultrasound, and the mixture was stirred at 80 °C for 40 min. A black precipitate was obtained after standing for 60 min. The precipitate was separated with an external magnetic field, and magnetic fluid Fe_3O_4 was obtained (Luo et al. 2010). In the second step, the magnetic fluid was dispersed with 500 mL of C_2H_5OH and 250 mL of deionised water with ultrasound for 10 min. Then, 38 mL $NH_3{\cdot}H_2O$ and 50 mL ethyl orthosilicate were added and the mixture was agitated at 60 °C for 4.5 h. Fe_3O_4@Si–OH was obtained by magnetic separation. In the third step, the Fe_3O_4@Si–OH magnetic nanoparticles (0.20 g) were dispersed in a chitosan solution (60 mL, 1%). The optimal amount of glutaraldehyde (Fig. S1) was determined by gradually adding 3-mL portions of glutaraldehyde solution (5%) with stirring. The mixture was stirred at 60 °C for 30 min. The products were separated with an external magnetic field, washed with acetic acid (3%), and dried at 80 °C. Fe_3O_4@Si–OH@CS-Glu was obtained and stored at 25℃.

Characterisation

The conductive adhesive was coated on the surface of the sample in a vacuum environment, and the adsorbent was observed by scanning electron microscopy (SEM) with

SU-1510 (Japan) at a voltage of 5 kV. The X-ray diffraction (XRD) patterns were measured at 100 mA in the 2θ range of 5°–80° with a Smartlab (Neo-Confucianism, Japan) using Cu Kα radiation. A Nicolet Nexus 6700 FTIR (USA) spectrometer was used to determine the Fourier transform infrared (FTIR) spectra of the Fe_3O_4, Fe_3O_4@Si–OH, Fe_3O_4@Si–OH@CS-Glu, and chitosan solution (1%) samples in the region between 400 and 4000 cm^{-1}. At 243.15 K, a Belsorp Max nitrogen gas adsorption analyser (BLE, USA) was used to determine the pore size, specific surface area, and pore volume of the adsorbent surface by nitrogen adsorption–desorption analysis using the Brunauer–Emmett–Teller (BET) method. The surface potentials (zeta) of Fe_3O_4@Si–OH and Fe_3O_4@Si–OH@CS-Glu were measured using a nanoparticle potentiometer (Zetasizer Nano ZS90, Malvern, UK). A Versalab vibrating sample magnetometer (VSM, Quantum Design, USA) was used to measure the magnetisation of the adsorbents.

Batch adsorption experiments

We use the single factor method to optimise. First, 1 mL of Cr(VI) (20 µg/mL) solution and 50 mg of adsorbent were mixed in a 5-mL centrifuge tube for batch adsorption experiments. In addition to exploring the factors influencing pH, other adsorption experiments were carried out with a pH of 2.5. To explore the effect of pH on adsorption efficiency, 0.1 M HCl and NaOH (0.1 M) were used to adjust the pH value of Cr(VI) from 1.0 to 7.0. The effect of adsorbent dosage on the adsorption efficiency was investigated by changing the amount of adsorbent from 25 to 150 mg. The effect of adsorption time was studied by changing the adsorption time from 5 to 90 min. To study the adsorption efficiency of the adsorbent with heavy metal ions, the concentrations for each heavy metal were selected according to the national standard method (GB/T 5750.12–2006); 20 µg/L As^{5+}, 1 µg/L Hg^{2+}, 50 µg/L Se^{6+}, 40 µg/L Pb^{2+}, and 7 µg/L Cd^{2+} were used for adsorption. To study the adsorption capacity of the adsorbent on heavy metal ions, 50 mg of Fe_3O_4@Si–OH@CS-Glu was added, and the concentrations of Cr(VI), As^{5+}, Hg^{2+}, and Se^{6+} were changed from 0 to 800 mg/L. Furthermore, 200 µg/L Cr(VI), 20 µg/L As^{5+}, 1 µg/L Hg^{2+}, and 50 µg/L Se^{6+} were used for the cation adsorption competition experiments. The concentration of Cr(VI) was determined using a UV/visible spectrophotometer (UV-2550, Tianjin, China). The concentrations of As^{5+}, Hg^{2+}, and Se^{6+} were determined using an atomic fluorescence photometer (AFS-930, Beijing Jitian Instrument Co., Ltd., China). The adsorption capacity of the adsorbents for heavy metal ions q_e (mg/g) and the removal percentage η (%) were determined based on the following equations:

$$q_e = \frac{(C_0 - C_e)V}{m} \tag{1}$$

$$\eta = \frac{(C_0 - C_e)}{C_0} \times 100\% \tag{2}$$

where q_e (mg/g) is the adsorption capacity of heavy metals, C_0 (µg/L) is the initial concentration of heavy metal ions, C_e (µg/L) is the equilibrium concentration of heavy metal ions, V (mL) is the volume of the adsorbate solution, m (mg) is the amount of adsorbent, and η (%) is the percentage of heavy metal ions adsorbed from the solution.

Fe_3O_4@Si–OH@CS-Glu application for bacteria

Escherichia coli was cultured in accordance with the standard test method (GB/T 5750.12–2006). Nutritional AGAR medium was used instead of beef extract peptone medium to reduce the pH adjustment steps. First, 2.5 mg Fe_3O_4@Si–OH@CS-Glu was added to a certain volume of bacterial liquid for vibration adsorption. After magnetic separation, 200 µL of the supernatant was collected and coated on a plate. This step was carried out in a biosafety cabinet. The coated plate was then placed in an electric thermostatic incubator and cultured at 37 °C for 24–48 h. The number of colonies that grew on each plate was counted. Finally, 200 µL of bacterial solution (diluted 1000 times) was coated onto the plate to calculate the blank colony. This step was carried out in a biosafety cabinet. The adsorption rate (*AR*) was calculated using the following equation:

$$AR = \frac{N_a}{N_0} \tag{3}$$

where *AR* indicates the removal efficiency (%), N_a is the number of bacteria after adsorption, and N_0 is the number of bacteria in the control group.

Results and discussions

Characterisation of adsorbents

The synthesis of Fe_3O_4@Si–OH@CS-Glu involves three steps (Fig. S2). SEM and SEM mapping were used to characterise the size, shape, and surface element distribution of Fe_3O_4, Fe_3O_4@Si–OH, and Fe_3O_4@Si–OH@CS-Glu. As shown in Fig. 1 (a), Fe_3O_4 has an irregular blocky structure. In Fig. 1 (b), Fe_3O_4@Si–OH exhibits a regular spherical structure with a smooth surface and a particle size of approximately 125 nm, possibly because Si–OH is coated on the surface of Fe_3O_4. As shown in Fig. 1 (c), the approximately 170 nm particle size of Fe_3O_4@Si–OH@CS-Glu was greater than that of Fe_3O_4@

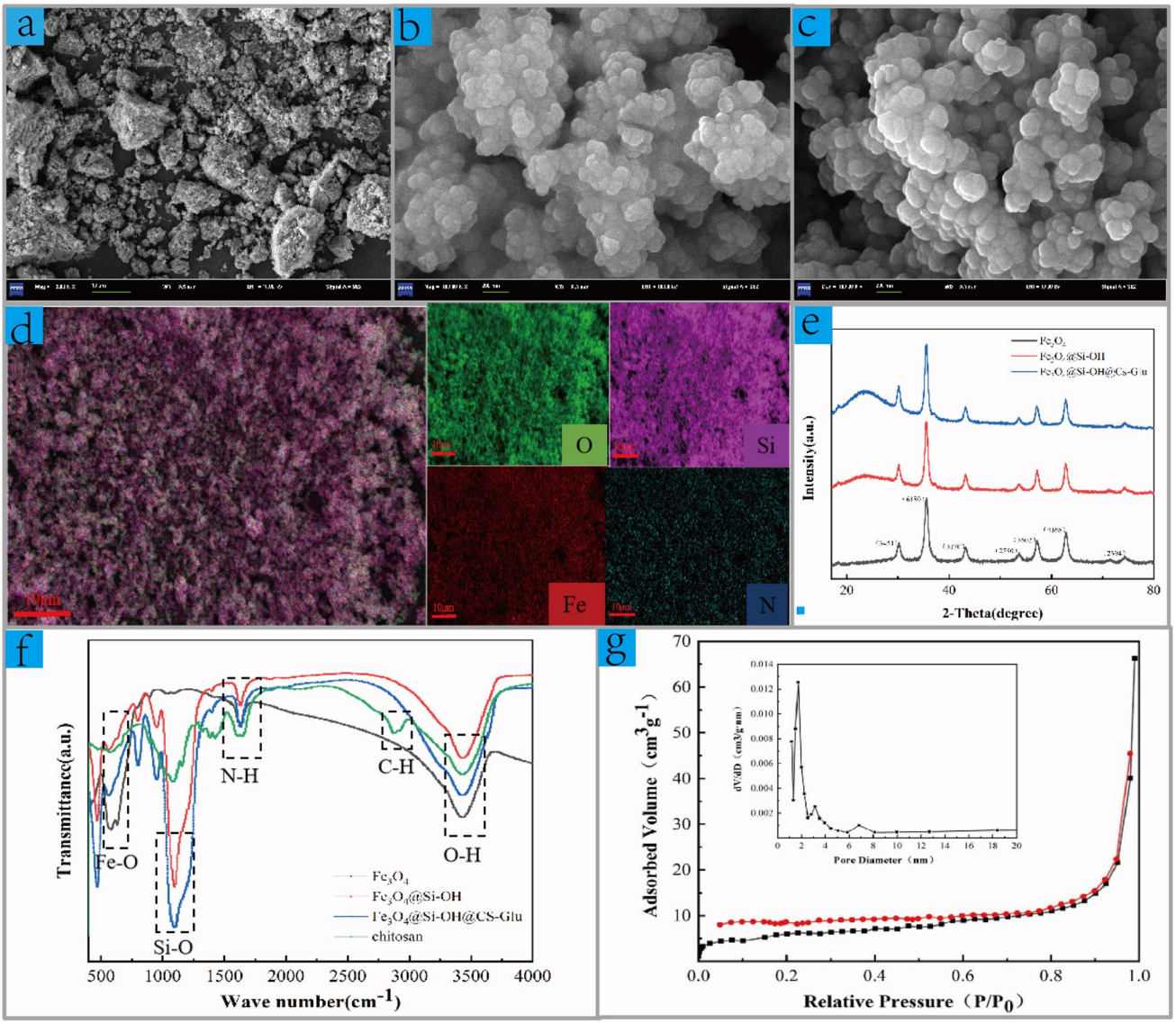

Fig. 1 SEM images of (**a**) Fe_3O_4, (**b**) Fe_3O_4@Si–OH, and (**c**) Fe_3O_4@Si–OH@CS-Glu. (**d**) SEM mapping image of Fe_3O_4@Si–OH@CS-Glu. (**e**) XRD patterns of Fe_3O_4, Fe_3O_4@Si–OH, and Fe_3O_4@Si–OH@CS-Glu. (**f**) FTIR spectra of Fe_3O_4, Fe_3O_4@Si–OH, Fe_3O_4@Si–OH@CS-Glu, and chitosan. (**g**) N_2 adsorption–desorption isotherms of Fe_3O_4@Si–OH@CS-Glu (inset: Barrett–Joyner–Halenda (BJH) pore size distribution)

Si–OH. Fe_3O_4@Si–OH@CS-Glu exhibited an agglomeration phenomenon, which may be caused by the uneven dispersion of chitosan. Because the dose of Fe_3O_4@Si–OH@CS-Glu in the experiments was sufficient, the mild agglomeration does not affect the adsorption performance. The local elemental information of Fe_3O_4@Si–OH@CS-Glu is shown in Fig. 1 (d). The results show that Fe, O, Si, and N are uniformly distributed on the surface of Fe_3O_4@Si–OH@CS-Glu, indicating that Si–OH and CS-Glu coated Fe_3O_4 successfully.

The crystal structure and integrity of the adsorbents were determined using XRD patterns. Figure 1 (e) shows the XRD patterns of Fe_3O_4, Fe_3O_4@Si–OH, and Fe_3O_4@Si–OH@CS-Glu. The diffraction peaks at 30.3°, 35.5°, 43.1°, 53.7°, 57.2°, 62.8°, and 72.9° have intensities of (3451), (6480), (3170), (2780), (3602), (4168), and (2394) respectively. This indicates that Fe_3O_4 is present as a cubic phase with a face-centred cubic structure (JCPDS card no. 19–0629) and exists as a stable phase throughout the synthesis process. The peak value of 2θ increased between 20 and 70°, which was likely the result of the amorphous Si–OH coating on Fe_3O_4. The peaks for Fe_3O_4@Si–OH@CS-Glu broadened at 20° and 30°, which may be attributed to the addition of chitosan. Therefore, Fe_3O_4 was successfully coated with Si–OH and CS-Glu.

The chemical functional groups on the surface of Fe_3O_4, Fe_3O_4@Si–OH, Fe_3O_4@Si–OH@CS-Glu, and chitosan in the 400–4000 cm^{-1} region were determined using Fourier transform infrared spectroscopy (FTIR). As shown in Fig. 1 (f), Fe–O stretching vibration peaks can be observed at 583 cm^{-1} in Fe_3O_4, Fe_3O_4@Si–OH, and Fe_3O_4@Si–OH@CS-Glu (Lei et al. 2020). The peak value of 2880 cm^{-1} was caused by the vibration of the C-H bond contraction. The vibration absorption peak of the O–H bond in water is 3440 cm^{-1} (Lu et al. 2013). The peak at 1100 cm^{-1} was caused by the stretching vibration of the Si–O bond (Zhang et al. 2015). This indicates that Si–OH successfully coated the surface of Fe_3O_4. At 1620 cm^{-1}, the vibration absorption peak of N–H in chitosan was observed, indicating that Fe_3O_4@Si–OH was successfully modified with CS-Glu (Gedam and Dongre 2015).

The BET and Barrett–Joyner–Halenda (BJH) methods were used to analyse the specific surface area, pore volume, and pore size of the adsorbents with N_2 desorption and adsorption isotherms. As shown in Fig. 1 (g), a typical characteristic of the type III isotherm is that it is accompanied by an H3 type hysteresis loop, indicating that Fe_3O_4@Si–OH@CS-Glu is a mesoporous material (Kruk and Jaroniec 2001). The pore parameters of the three materials are listed in Table S1. The specific surface area of Fe_3O_4 is 141.86 m^2/g, which is favourable for Si–OH coating. The specific surface area of Fe_3O_4@Si–OH is 21.82 m^2/g, possibly due to the addition of Si–OH to the Fe_3O_4 surface. The specific surface area of Fe_3O_4@Si–OH@CS-Glu is 27.34 m^2/g, indicating no significant change from that of Fe_3O_4@Si–OH. The modification of CS-Glu did not increase the specific surface area of the material.

The zeta potential was used to determine the charge type on the surface of the adsorbent. As shown in Fig. S3, the surface of Fe_3O_4@Si–OH was negatively charged (−41.3 mV), which may have resulted from the addition of Si–OH to the surface of Fe_3O_4@Si–OH. However, the surface of Fe_3O_4@Si–OH@CS-Glu was positively charged (+28.89 mV), indicating that -NH_2 successfully modified Fe_3O_4@Si–OH, making it more conducive to electrostatic adsorption.

The magnetic properties of the three materials were studied by examining their magnetic hysteresis loops. As seen in Fig. S4, the remanent magnetism and coercivity of these three materials are close to zero, indicating that they have superparamagnetic properties (Cheng et al. 2018). The saturation magnetisations of Fe_3O_4, Fe_3O_4@Si–OH, and Fe_3O_4@Si–OH@CS-Glu were 84.2 emu/g, 76.4 emu/g, and 57.8 emu/g, respectively. The decrease in saturation magnetisation may be due to the addition of non-magnetic Si–OH and CS-Glu. Although the magnetic field intensity of Fe_3O_4@Si–OH@CS-Glu was lower, it was high enough to facilitate rapid separateion under an applied magnetic field (Fig. S4 Inset). Therefore, the adsorbent can be rapidly separated from the solution using an external magnetic field (Huang and Chen 2009).

Adsorption of heavy metals

Effect of pH

The pH is a significant factor that can affect adsorption efficiency. Most heavy metal ions exist in water in the form of oxyanions, which will electrostatically adsorb with positively charged adsorbents on the surface. Cr(VI) was selected as the model heavy metal for further condition optimisation of the conditions. As shown in Fig. 2 (a), the removal efficiency increased from 27 to 80% when the pH changed from 1 to 2.5. When the pH was changed from 2.5 to 7, removal efficiency was decreased to 8.5%. This is mainly because the -NH_2 on the surface of Fe_3O_4@SiO_2@CS-Flu gets protonated by the amino group under acidic conditions, which makes the adsorbent surface positively charged. Under acidic conditions, Cr(VI) mainly exists in the anion form of H_2CrO_4 and $HCrO_4^-$. The concentration of $HCrO_4^-$ increased with increasing pH. Less Cr(VI) exists in the form of anions when the pH is lower than 2.5,

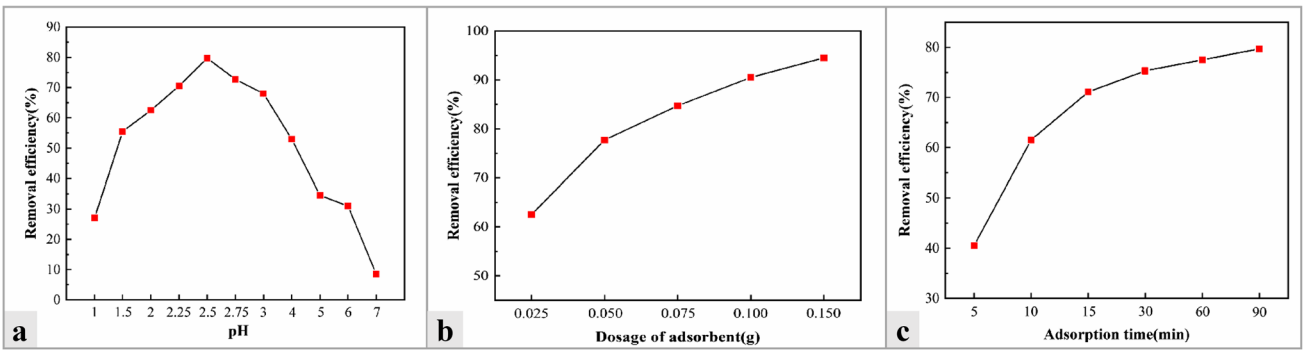

Fig. 2 Effect of (**a**) pH, (**b**) contact time, and (**c**) amount of adsorbent on adsorption efficiency

which resulting in a low adsorption efficiency (Jiang et al. 2019). However, the number of protonated amino groups decreases with increasing pH. The positive charge was weakened at higher pH, which resulting in reduced adsorption capacity (Lei et al. 2020). In addition, it was noted that cross-linking of CS forms a network structure with good water solubility, which not only facilitates the entry of water into the gel network but also facilitates the interaction between Cr(VI) ions and the active groups of CS. It has proudced the good adsorption performance (Jawad et al. 2020a, 2020b, 2020c). Therefore, a pH of 2.5 was selected for further experiments.

Effect of adsorption time

The adsorption time influenced the adsorption equilibrium between the adsorbents and the targets. Figure 2 (b) shows the relationship between the adsorption time and the adsorption efficiency. The adsorption efficiency increased rapidly when the adsorption time was below 15 min. This may be due to the fact that the surface of adsorbents can initially provide a large number of adsorption sites for targets. When the adsorption time was changed from 15 to 90 min, the adsorption efficiency increased slowly. This may have been due to a large number of occupied active sites on the surface of the adsorbent as well as complexation playing a dominant role. The process was slow, and the maximum adsorption capacity was 82.5 mg/g after adsorption for 180 min of adsorption (Zhou et al. 2019). In consideration of this and other factors of time cost and adsorption efficiency, an adsorption time of 15 min was selected.

Effect of absorbent dosage

The weight of the adsorbent make it suitable for adsorption and elution. Figure 2 (c) shows the relationship between the absorbent dosage and the adsorption efficiency. The adsorption efficiency increased from 62.5 to 90.5% when the adsorbent dosage was increased from 25 mg to 100 mg. This is because the adsorption sites increase with increasing adsorbent dosage. Moreover, the adsorption efficiency increased from 90.5 to 94.5% when the adsorbent dosage was increased from 100 to 150 mg. This slight increase in efficiency may be due to the decreased mass ratio of adsorbent to Cr(VI) with the increased dosage of adsorbent, which leads to the under-utilisation of Fe_3O_4@Si–OH@CS-Glu surface adsorption sites (Zeng et al. 2020). Based on our results, we inferred that a good adsorption efficiency can be achieved with 100 mg of adsorbents.

Adsorption of other heavy metals

Various heavy metal ions present in water pose severe risks to environmental and public health. Therefore, the ability of materials to remove multiple types of heavy metal ions is very important for practical applications. The adsorption efficiencies of Fe_3O_4@Si–OH@CS-Glu for several typical heavy metals, including As^{5+}, Hg^{2+}, and Se^{6+}, were further studied. As shown in Fig. 3 (a), the proposed material also exhibited excellent adsorption performance under the optimum adsorption conditions for Cr(VI). The adsorption efficiencies for As^{5+}, Hg^{2+}, and Se^{6+} were 73.5%, 91.6%, and 100.0%, respectively. However, the removal efficiency of this adsorbent for Pb^{2+} and Cd^{2+} was not as high as others. Cd^{2+} and Pb^{2+} mainly exist in the form of cations in water. The low removal rate of these metals may be due to their surface charges. Under the optimum adsorption conditions for Cr(VI), the adsorption capacities of Fe_3O_4@Si–OH@CS-Glu for Cr(VI), As^{5+}, Hg^{2+}, and Se^{6+} were also studied. As shown in Fig. 3 (b), adsorption capacity is not directly proportional to adsorption efficiency. The adsorption of heavy metals by chitosan is consistent with the Langmuir adsorption isotherm and pseudo-second-order kinetic model, indicating that the adsorption is a monolayer and chemical bonding is dominant (Saheed et al. 2020). As shown in Table S2, the adsorption capacity of Fe_3O_4@Si–OH@CS-Glu for heavy metals was

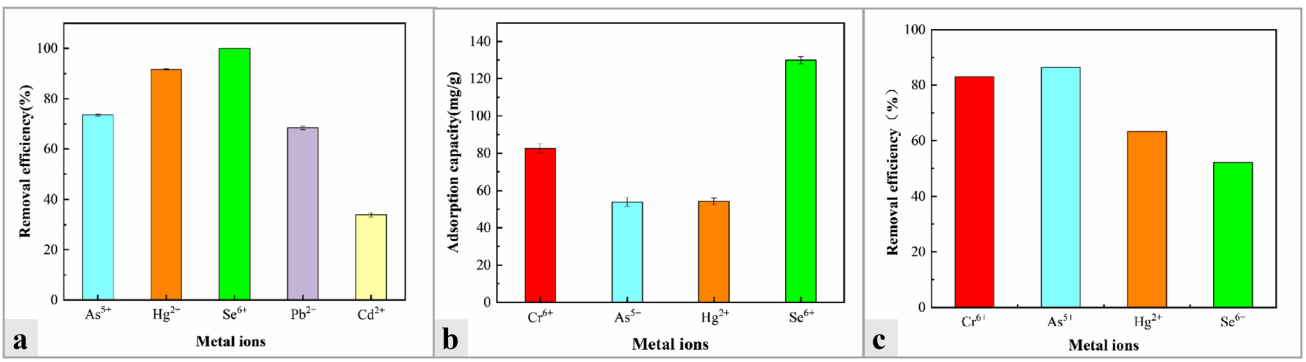

Fig. 3 **a** Adsorption efficiency of adsorbents for other heavy metals. **b** Adsorption capacity of adsorbents for Cr(VI), As^{5+}, Hg^{2+}, and Se^{6+}. **c** Adsorption efficiency of adsorbents with cationic competition between multiple heavy metals

also higher than that of other materials reported in the literature (Popovic et al. 2020). Therefore, Fe_3O_4@Si–OH@CS-Glu can potentially be applied for the simultaneous removal and enrichment of heavy metal ions.

Effect of competing metal ions

When multiple metal ions coexist in the environment, the adsorption capacity of the adsorbent may be reduced, because they compete with each other for the adsorption site. Therefore, a series of metal cations were selected as research objects to explore the order in which heavy metals are adsorbed by Fe_3O_4@Si–OH@CS-Glu. The adsorption efficiency of Fe_3O_4@Si–OH@CS-Glu for various metal cations was also studied. As shown in Fig. 3 (c), when Cr(VI), As^{5+}, Hg^{2+}, and Se^{6+} coexist, the adsorption efficiency of Cr(VI) ≈ As^{5+} > Hg^{2+} > Se^{6+}, which differs from that for single metal ions. According to the literature (Huang et al. 2019), both Cr(VI) and As exist in the form of typical oxygen anions ($HCrO_4^-$, $H_2AsO_4^-$, and $HAsO_4^{2-}$) under acidic conditions (Zhang et al. 2016). Oxygen anions exhibit preferential electrostatic adsorption with protonated amino groups on the surface of Fe_3O_4@Si–OH@CS-Glu. Therefore, the adsorption efficiencies for Cr(VI) and As^{5+} were higher than those for Hg^{2+} and Se^{6+}, when they all four metals were coexisting.

Adsorption of bacteria

Effect of pH

Antibiotic resistance, especially that of gram-negative bacteria, is one of the greatest public health threats worldwide. Moreover, as the most significant microbial habitat, aquatic environments are known to be favourable for antibiotic gene transfer. They reportedly play a crucial role in the spread of drug resistance in an environment (Cherak et al. 2021). The adsorption ability of Fe_3O_4@Si–OH @CS-Glu for *E. coli* was evaluated, as a typical representative of gram-negative bacteria. First, the pH of the system was optimised. As shown in Fig. 4 (a), Fe_3O_4@Si–OH@CS-Glu demonstrated sufficient adsorption of *E. coli* under pH levels of 3.0 to 9.0. The surface of Fe_3O_4@Si–OH@CS-Glu is positively charged due to the protonation of amino group. The cell membrane surface and cytoplasm of *E. coli* are negatively charged. There are two mechanisms on the removal of *E. coli* by the adsorbent. For the first mechanism, the adsorbent was adsorbed on the cell membrane to form a polymer film at pH 3, which inhibiting the entry of nutrients into *E. coli* through the cell membrane. For the second mechanism, low molecular chitosan entered the cell membrane and was electrostatically adsorbed by the cytoplasm when pH values were higher than 5.0, which leads to the apoptosis of *E. coli* (Lin et al. 2018).

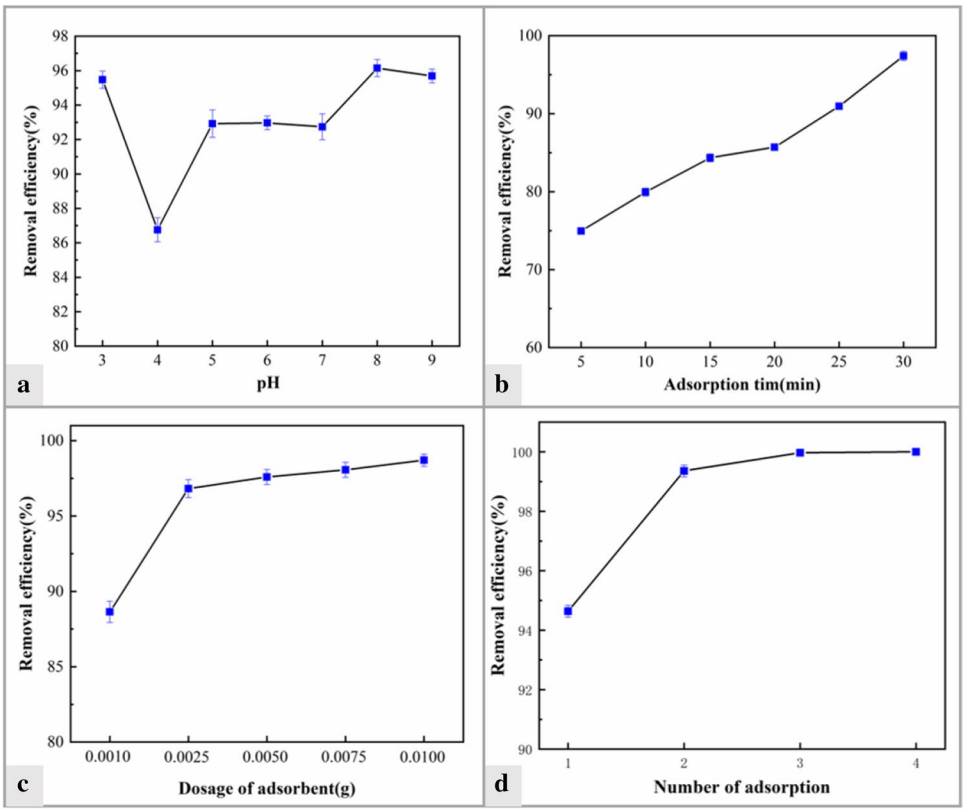

Fig. 4 **a** Removal efficiency for *Escherichia coli* at various pH levels. **b** Removal efficiency for *E. coli*. with different absorption times. **c** Effect of adsorbent dosage on the adsorption efficiency for *E. coli*. **d** The effects of different adsorption times on the adsorption efficiency for *E. coli*

The adsorption efficiency of Fe_3O_4@Si–OH@CS-Glu for *E. coli* was increased from 92.92 to 96.15%. When pH value was 4, it was the junction of two mechanisms which leads to lower removal efficiency.

Effect of adsorption time

The adsorption time plays an important role in practical applications. As shown in Fig. 4 (b), when the amount of magnetic material was 1.0 mg and the adsorption time was 5 min, the removal efficiencies had reached 74.95%. When the adsorption time was changed from 10 to 30 min, the adsorption efficiencies changed from 79.95 to 97.41%. During the initial 5 min, the *E. coli* were fast adsorbed on the surface of Fe_3O_4@Si–OH@CS-Glu. The adsorption rate was decreased after 5 min, which proved the most surface of Fe_3O_4@Si–OH@CS-Glu had been covered by lots of *E. coli*. Combined the removal efficiency and adsorption time, 5 min was selected as a practical adsorption time for further experiments. The dosage of adsorbent was further optimised in the next experiment.

Effect of adsorbent dosage

The adsorption sites of Fe_3O_4@Si–OH@CS-Glu increased with increasing adsorbent dosage. Various dosages of Fe_3O_4@Si–OH@CS-Glu were studied, namely 0.001 g, 0.0025 g, 0.005 g, 0.0075 g, and 0.01 g (Fig. 4(c)). The initial concentration of *E. coli* was 656,500 CFU/mL, and the adsorption time was 5 min. With 0.001 g of Fe_3O_4@Si–OH@CS-Glu, the adsorption efficiency reached 88.4%. When the dosage of adsorbent was changed from 0.0025 to 0.01 g, the adsorption efficiency was further increased from 96.82 to approximately 100%. During the process, the removal efficiency was increased rapidly with the increase of adsorbent dosage. The results indicated that 0.001 g adsorbent was insufficient. When the dosage of adsorbent was greater than 0.0025 g, the adsorbent was sufficient. The removal efficiency had shown a slow increase when the dosage of adsorbent was increased. Therefore, 0.0025 g adsorbent was selected for further experiment.

Effect of repeated treatments

As reported in the literature, all active sites on the material become occupied when a large number of bacteria are present in the samples, and excessive bacterial fluid cannot be adsorbed (Rihayat et al. 2020). Therefore, an experiment was conducted with multiple doses of 0.0025 g of adsorbent. As shown in Fig. 4 (d), the adsorption efficiency was 94.6%

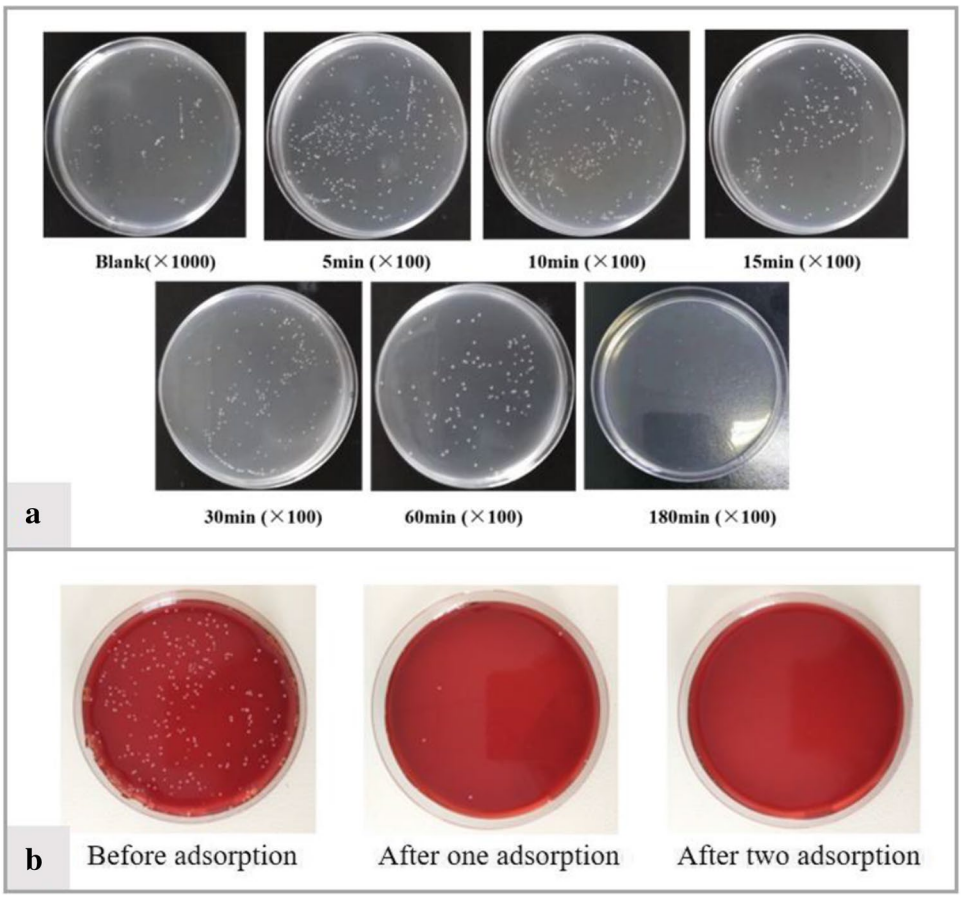

Fig. 5 **a** Adsorption of *Escherichia coli* by adsorbent. **b** Adsorption of *Staphylococcus aureus* by adsorbent

at an adsorption time of 5 min when the concentration of *E. coli* was 451,500 CFU/mL. The adsorption efficiency was 99.36% after two adsorption cycles, which was higher than the adsorption efficiency of 0.005 g adsorbent for one time adsorption (Fig. 4 (c)). The adsorption efficiency was about 100% after four adsorption cycles. Therefore, the proposed materials can be used to efficiently remove bacteria through repeated adsorption.

Adsorption of gram-positive bacterium

The performance of the proposed materials was also verified for gram-positive bacteria. *Staphylococcus aureus* is a typical gram-positive bacterium. It can cause various illnesses, from minor skin infections to life-threatening diseases (Tong et al. 2010). Moreover, *S. aureus* is widespread in the environment, including air and sewage. Therefore, *S. aureus* was used as a model bacterium to demonstrate this adsorption method. As shown in Fig. 5 (b), under the optimal conditions for *E. coli*, the proposed material also showed excellent adsorption and removal performance for *S. aureus*. With a 5-min adsorption time and 25 mg of adsorbent, *S. aureus* could be removed completely after two adsorption cycles, because the isoelectric point of most gram-positive bacteria was estimated to be 2–3, which was lower than that of gram-positive bacteria. But different from *E. coli*, the first adsorption mechanism played a dominant role on the removal of *S. aureus* by Fe_3O_4@Si–OH@CS-Glu. The proposed adsorption method showed a good adsorption performance and can be used for the complete removal of gram-positive bacteria.

Conclusions

In conclusion, we developed a magnetic adsorbent (Fe_3O_4@Si–OH@CS-Glu) by combining chitosan-silanol groups with glutaraldehyde as a cross-linking agent. Under the optimum condition, the removal efficiencies of Fe_3O_4@Si–OH@CS-Glu for Cr^{6+}, As^{5+}, Hg^{2+}, and Se^{6+} were as high as 90.5%, 73.5%, 91.6%, and 100.0% respectively. In addition, the adsorbent has shown excellent the adsorption capacity for heavy metals compared with reported other materials in the literature. When multiple heavy metal ions coexist, the magnetic adsorbent preferentially adsorbs Cr^{6+} and As^{5+}. Moreover, in the pH range of 3–9, *E. coli* (gram-negative) and *S. aureus* (gram-positive) can be removed after 2–4 adsorption cycles with 2.5 mg Fe_3O_4@Si–OH@CS-Glu. The adsorbent is easy to be synthesised with high adsorption performance. It is expected to be an effective adsorbent for the removal of heavy metals and bacteria from the contaminated water.

Supplementary Information The online version contains supplementary material available at https://doi.org/10.1007/s11356-022-20673-5.

Author contribution Huanying Zhou and Zhangrun Xu conceived the project. Tie Han and Zhixian Gao prepared all the materials for experiments and characterizations. Shuyue Ren and Shuang Li performed data analysis. Xueli Liu, Yonghui Wang, and Qibo Liu summarised all data and drafted the manuscript. All authors discussed the results and commented on the manuscript.

Funding This study was supported by the National Key R&D Program of China (grant no. 2017YFC1601101). The funders played no role in study design, collection, analysis, or interpretation of data, the writing of the report, or the decision to submit the article for publication.

Declarations

Ethics approval Not applicable.

Consent to participate Yes.

Consent for publication Yes.

Competing interests The authors declare no competing interests.

References

Abdulhameed AS, Mohammad A, Jawad AH (2019) Application of response surface methodology for enhanced synthesis of chitosan tripolyphosphate/TiO_2 nanocomposite and adsorption of reactive orange 16 dye[J]. J Clean Prod 232:43–56. https://doi.org/10.1016/j.jclepro.2019.05.291

Ahj A, Nsam A, Asa B (2020) Tunable Schiff's base-cross-linked chitosan composite for the removal of reactive red 120 dye: adsorption and mechanism study - ScienceDirect[J]. Int J Biol Macromol 142:732–741. https://doi.org/10.1016/j.ijbiomac.2019.10.014

Ahj A, Uks A, Naj A, Zaa B, Ldw C (2021) Magnetic crosslinked chitosan-tripolyphosphate/MgO/ Fe_3O_4 nanocomposite for reactive blue 19 dye removal: optimization using desirability function approach. Surf Interfaces 28:101698. https://doi.org/10.1016/j.surfin.2021.101698

Allen C, Cheng, Bart J, Currie (2007) Melioidosis: epidemiology, pathophysiology, and management. Clin Microbiol Rev 18(2):383–416. https://doi.org/10.1128/CMR.00018-07

Altun E, Elik E, Ersan HY (2020) Tailoring the microbial community for improving the biodegradation of chitosan films in composting environment. J Polym Environ 28(5):1548–1559. https://doi.org/10.1007/s10924-020-01711-0

Anwar M, Muhammad F, Akhtar B, Rehman SU, Saleemi MK (2020) Nephroprotective effects of curcumin loaded chitosan nanoparticles in cypermethrin induced renal toxicity in rabbits. Environ Sci Pollut Res 27(13):14771–14779. https://doi.org/10.1007/s11356-020-08051-5

Bairagi S, Ali SW (2020). Conventional and advanced technologies for wastewater treatment. Environ Nanotechnology Water Purif 33-56https://doi.org/10.1002/9781119641353.ch2

Cheng M-A, Wang Z-A, Lv Q-A et al (2018) Preparation of amino-functionalized Fe_3O_4@mSiO_2 core-shell magnetic nanoparticles and their application for aqueous Fe^{3+} removal. J Hazard Mater 341:198–206. https://doi.org/10.1016/j.jhazmat.2017.07.062

Chen W-H, Huang J-R (2020) Adsorption of organic including pharmaceutical and inorganic contaminants in water toward

graphene-based materials. Contan Emerg Concern Water and Wastewater 93–113. https://doi.org/10.1016/B978-0-12-813561-7.00003-1

Cherak Z, Loucif L, Moussi A, Rolain JM (2021) Carbapenemase producing Gram-negative bacteria in aquatic environments: a review. J Glob Antimicrob Resist. https://doi.org/10.1016/j.jgar.2021.03.024

Dehaghi SM, Rahmanifar B, Moradi AM, Azar PA (2014) Removal of permethrin pesticide from water by chitosan–zinc oxide nanoparticles composite as an adsorbent. J Saudi Chem Soc 18(4):348–355. https://doi.org/10.1016/j.jscs.2014.01.004

Dobrzyńska J (2021) Amine-and thiol-functionalized SBA-15: potential materials for As (V), Cr (VI) and Se (VI) removal from water. Comparative Study. J Water Process Eng 40:101942. https://doi.org/10.1016/j.jwpe.2021.101942

Gabriel SK, Peters L, Mucalo M (2020) Chitosan: a review of sources and preparation methods. Int J Biol Macromol 169:85–94. https://doi.org/10.1016/j.ijbiomac.2020.12.005

Gedam AH, Dongre RS (2015) Adsorption characterization of pb(II) ions onto iodate doped chitosan composite: equilibrium and kinetic studies. RSC Adv 5(67):54188–54201. https://doi.org/10.1039/c5ra09899h

Gothandam KM, Ranjan S, Dasgupta N, Lichtfouse E (2020) Environmental chemistry for a sustainable world. Environ Biotechnol 2:45. https://doi.org/10.1007/978-3-030-381967

Guo X, Du B, Wei Q, Yang J, Hu L, Yan L, Xu W (2014) Synthesis of amino functionalized magnetic graphenes composite material and its application to remove Cr(VI), Pb(II), Hg(II), Cd(II) and Ni(II) from contaminated water. J Hazard Mater 278:211–220. https://doi.org/10.1016/j.jhazmat.2014.05.075

Habiba U, Siddique TA, Tan CJ, Salleh A, Afifi AM (2017) Synthesis of chitosan/polyvinyl alcohol/zeolite composite for removal of methyl orange, congo red and chromium (VI) by flocculation/adsorption. Carbohyd Polym 157:1568. https://doi.org/10.1016/j.carbpol.2016.11.037

Hashim MA, Mukhopadhyay S, Sahu JN, Sengupta B (2011) Remediation technologies for heavy metal contaminated groundwater. J Environ Manage 92(10):2355–2388. https://doi.org/10.1016/j.jenvman.2011.06.009

Huang D, Wu J-Z et al (2019) Novel insight into adsorption and co-adsorption of heavy metal ions and an organic pollutant by magnetic graphene nanomaterials in water. Chem Eng J. https://doi.org/10.1016/j.cej.2018.10.138

Huang S, Chen D (2009) Rapid removal of heavy metal cations and anions from aqueous solutions by an amino-functionalized magnetic nano-adsorbent. J Hazard Mater 163:174–179. https://doi.org/10.1016/j.jhazmat.2008.06.075

Ince M, Kaplan-Ince O, Ondrasek G (2020) Heavy metal removal techniques using response surface methodology: water/wastewater treatment, Book: Toxic nanomater, Chapter 1. https://doi.org/10.5772/intechopen.85340(Chapter 1). https://doi.org/10.5772/intechopen.88915

Jawad AH, Abdulhameed AS, Abdallah R, Yaseen ZM (2020a) Zwitterion composite chitosan-epichlorohydrin/zeolite for adsorption of methylene blue and reactive red 120 dyes. Int J Biol Macromol 163(756–765):163. https://doi.org/10.1016/j.ijbiomac.2020.07.014

Jawad AH, Abdulhameed AS, Mastuli MS (2020b) Mesoporous crosslinked chitosan-activated charcoal composite for the removal of thionine cationic dye: comprehensive adsorption and mechanism study. J Polym Environ 28(3):1095–1105. https://doi.org/10.1007/s10924-020-01671-5

Jawad AH, Abdulhameed AS, Wilson LD, Hanafiah M, Khan MR (2021) Fabrication of Schiff's base chitosan-glutaraldehyde/activated charcoal composite for cationic dye removal: optimization using response surface methodology. J Polym Environ 29:2855–2868. https://doi.org/10.1007/s10924-021-02057-x

Jawad AH, Malek N, Abdulhameed AS et al (2020c) Synthesis of magnetic chitosan-fly Ash/Fe_3O_4 composite for adsorption of reactive orange 16 dye: optimization by Box-Behnken design[J]. J Polym Environ 28(3):1068–1082. https://doi.org/10.1007/s10924-020-01669-z

Jiang Y, Cai W, Tu W, Zhu M (2019) A facile crosslink method to synthesize magnetic Fe_3O_4@SiO_2-chitosan with high adsorption capacity toward hexavalent chromium. J Chem Eng Data 64(1):226–233. https://doi.org/10.1021/acs.jced.8b00738

Koo KN, Ismail AF, Othman MHD, Bidin N, Rahman MA (2019) Preparation and characterization of superparamagnetic magnetite (Fe_3O_4) nanoparticles: a short review. Malays J Fundam Appl 15(1):23–31. https://doi.org/10.11113/mjfas.v15n2019.1224

Kruk M, Jaroniec M (2001) Gas adsorption characterization of ordered organic-inorganic nanocomposite materials. Chem Mater 13:3169–3183. https://doi.org/10.1021/cm0101069

Lei C, Wang C, Chen W, He M, Huang B (2020) Polyaniline@magnetic chitosan nanomaterials for highly efficient simultaneous adsorption and in-situ chemical reduction of hexavalent chromium: removal efficacy and mechanisms. Sci Total Environ 733:139316. https://doi.org/10.1016/j.scitotenv.2020.139316

Leus K, Folens K, Nicomel NR et al (2018) Removal of arsenic and mercury species from water by covalent triazine framework encapsulated γ-Fe_2O_3 nanoparticles. J Hazard Mater 353:312–319. https://doi.org/10.1016/j.jhazmat.2018.04.027

Li Z, Li L, Hu D, Gao C, Xiong J, Jiang H, Li W (2019) Efficient removal of heavy metal ions and organic dyes with cucurbit uril-functionalized chitosan. J Colloid Interface Sci 539:400–413. https://doi.org/10.1016/j.jcis.2018.12.078

Lin J, Song T, Liu Y, Yang J, Shu X, Li W-R, Chen J, Qiu X, Shi Q (2018) Preparation of modified silica/silver nanoparticles and its antibacterial properties. Ind Microbiol 48(05):19–22. https://doi.org/10.3969/j.issn.1001-6678

Liu X, Chuang M-A, Fan W-U et al (2019) Adsorption of Cr(VI) on chitosan/magnetic bagasse biochar composite material[J]. Hydrometallurgy 38(03):208–214. https://doi.org/10.13355/j.cnki.sfyj.2019.03.008

Lu B-Q, Zhu Y-J, Zhao X-Y, Cheng G-F, Ruan Y-J (2013) Sodium polyacrylate modified Fe_3O_4 magnetic microspheres formed by self-assembly of nanocrystals and their applications. Mater Res Bull 48(2). https://doi.org/10.1016/j.materresbull.2012.11.078

Luo B, Song X-J, Zhang F, Xia A, Yang W-L, Hu J-H, Wang C-C (2010) Multi-functional thermosensitive composite microspheres with high magnetic susceptibility based on magnetite colloidal nanoparticle clusters. Am Chem Soc 26(3):1674–1679. https://doi.org/10.1021/la902635k

Malek N, Jawad AH, Abdulhameed AS, Ismail K, Hameed BH (2020) New magnetic Schiff's base-chitosan-glyoxal/fly ash/fe_3O_4 biocomposite for the removal of anionic azo dye: an optimized process. Int J Biol Mmcromol 146:530–539. https://doi.org/10.1016/j.ijbiomac.2020.01.020

Mohammad AT, Abdulhameed AS, Jawad AH (2019) BoxBehnken design to optimize the synthesis of new crosslinked chitosan-glyoxal/TiO_2 nanocomposite: methyl orange adsorption and mechanism studies. Int J Biol Macromol 129:98–109. https://doi.org/10.1016/j.ijbiomac.2019.02.025

Mortazavi V, Nahrkhalaji MM, Fathi MH, Mousavi SB, Esfahani BN (2010) Antibacterial effects of sol-gel-derived bioactive glass nanoparticle on aerobic bacteria. J Biomed Mater Res 94(1):160–168. https://doi.org/10.1002/jbm.a.32678

Na G, Zhang W, Gao H, Wang C, Li R, Zhao F, Hou C (2021) Occurrence and antibacterial resistance of culturable antibiotic-resistant bacteria in the Fildes Peninsula. Antarctica Mar Pollut Bull 162:111829. https://doi.org/10.1016/j.marpolbul.2020.111829

Nawaz T, Zulfiqar S, Sarwar MI, Iqbal M (2020) Synthesis of diglycolic acid functionalized core-shell silica coated Fe_3O_4

nanomaterials for magnetic extraction of Pb(II) and Cr (VI) ions. Sci Rep 10(1):10076. https://doi.org/10.1038/s41598-020-67168-2

Nayak V, Jyothi MS, Balakrishna RG, Mahesh P, Ismail AF (2015) Preparation and characterization of chitosan thin films on mixed-matrix membranes for complete removal of chromium. Chemistry Open 4(3):278–287. https://doi.org/10.1002/open.201402133

Nishad PA, Bhaskarapillai A, Velmurugan S (2017) Enhancing the antimony sorption properties of nano titania-chitosan beads using epichlorohydrin as the crosslinker. J Hazard Mater 334:160–167. https://doi.org/10.1016/j.jhazmat.2017.04.009

Nnam A, Ahj A, Ki B, Rr A, Zaa C (2021) Fly ash modified magnetic chitosan-polyvinyl alcohol blend for reactive orange 16 dye removal: adsorption parametric optimization. Int J Biol Macromol 189:464–476. https://doi.org/10.1016/j.ijbiomac.2021.08.160

Panda L, Jena SK, Rath SS, Misra PK (2020) Heavy metal removal from water by adsorption using a low-cost geopolymer. Environ Sci Pollut Res 27:24284–24298. https://doi.org/10.1007/s11356-020-08482-0

Popovic AL, Rusmirovic JD, Velickovic Z, Radovanovic Z, Ristic M, Pavlovic VP, Marinkovic AD (2020) Novel amino-functionalized lignin microspheres: high performance biosorbent with enhanced capacity for heavy metal ion removal. Int J Biol Macromol 156:1160–1173. https://doi.org/10.1016/j.ijbiomac.2019.11.152

Reghioua A, Barkat D, Jawad AH et al (2021a) Magnetic chitosan-glutaraldehyde/zinc oxide/Fe_3O_4nanocomposite: optimization and adsorptive mechanism of remazol brilliant blue R dye removal. J Polym Environ 29:3932–3947. https://doi.org/10.1007/s10924-021-02160-z

Reghioua A, Barkat D, Jawad AH, Abdulhameed AS, Alothman ZA (2021b) Parametric optimization by Box-Behnken design for synthesis of magnetic chitosan-benzil/ZnO/Fe_3O_4 nanocomposite and textile dye removal. J Environ Chem Eng 9(13):105166. https://doi.org/10.1016/j.jece.2021.105166

Reghioua A, Barkat D, Jawad AH, Abdulhameed AS, Khan MR (2021c) Synthesis of Schiff's base magnetic crosslinked chitosan-glyoxal/ZnO/Fe_3O_4 nanoparticles for enhanced adsorption of organic dye: modeling and mechanism study. Sustain Chem Pharm 20(6):100379. https://doi.org/10.1016/j.scp.2021.100379

Reis, Rui L, Cohn, Daniel (2002) Polymer based systems on tissue engineering, replacement and regeneration: proceedings of the nato advanced study institute. Nato Sci 86:141–142. https://doi.org/10.1007/978-94-010-0305-6

Rihayat T, Suryani S, Riskina S, Nurhanifa N (2020) Synthesis and characterization of chitosan- bentonite modified polyurethane with biomedical potential. IOP Conf Series: Mater Sci Eng 830:042016. https://doi.org/10.1088/1757-899x/830/4/042016

Saheed IO, Da OW, Suah FB (2020) Chitosan modifications for adsorption of pollutants-a review. J Hazard Mater 408:124889. https://doi.org/10.1016/j.jhazmat.2020.124889

Sharma G, Naushad M et al (2016) Fabrication and characterization of chitosan-crosslinked-poly (alginic acid) nanohydrogel for adsorptive removal of Cr(VI) metal ion from aqueous medium. Int J Biol Macromol 95. https://doi.org/10.1016/j.ijbiomac.2016.11.072

Tang H-Z, Wang Y-H, Li S, Wu J, Li J-W, Zhou H-Y, Gao Z-X (2019) Graphene oxide composites for magnetic solid-phase extraction of twelve quinolones in water samples followed by MALDI-TOF MS. Anal Bioanal Chem 411:7039–7049. https://doi.org/10.1007/s00216-019-02081-w

Tanhaei B, Ayati A, Lahtinen M, Sillanp M (2015) Preparation and characterization of a novel chitosan/Al_2O_3/magnetite nanoparticles composite adsorbent for kinetic, thermodynamic and isotherm studies of methyl orange adsorption. Chem Eng J 259:1–10. https://doi.org/10.1016/j.cej.2014.07.109

Tong S, Shi R, Zhang H, Ma C (2010) Catalytic performance of Fe_3O_4-CoO/Al_2O_3 catalyst in ozonation of 2-(2,4-dichlorophenoxy) propionic acid, nitrobenzene and oxalic acid in water. J Environ Sci 22(10):1623–1628. https://doi.org/10.1016/S1001-0742(09)60298-9

Wang L, Huang X, Wang C et al (2020 Applications of surface functionalized Fe_3O_4 nps-based detection methods in food safety. Food Chem 128343. https://doi.org/10.1016/j.foodchem.2020.128343

Wu S-P, Dai X-Z, Kan J-R, Shi F-D, Zhu M-Y (2017) Fabrication of carboxymethyl chitosan– hemicellulose resin for adsorptive removal of heavy metals from wastewater. Chin Chem Lett 28(3):625–632. https://doi.org/10.1016/j.cclet.2016.11.015

Zeng H, Zhai L, Zhang J, Li D (2020) As(V) adsorption by a novel core-shell magnetic nanoparticles prepared with iron-containing water treatment residuals. Sci Total Environ 753:142002. https://doi.org/10.1016/j.scitotenv.2020.142002

Zhang B-Q, Chen N, Feng C-P, Zhang Z-Y (2018) Adsorption for phosphate by crosslinked/non-crosslinked-chitosan-Fe(III) complex sorbents: characteristic and mechanism. Chem Eng J 353:361–372. https://doi.org/10.1016/j.cej.2018.07.092

Zhang M-M, Liu Y-G, Li T-T, Xu W-H et al (2015) Chitosan modification of magnetic biochar produced from eichhornia crassipes for enhanced sorption of Cr(VI) from aqueous solution. RSC Adv 5(58):46955–46964. https://doi.org/10.1039/C5RA02388B

Zhang Y, Ye Y, Liu Z, Li B, Liu Q-Z, Liu Q-C, Li X (2016) Monodispersed hierarchical aluminum/iron oxides composites micro/nanoflflowers for effifficient removal of As(V) and Cr(VI) ions from water. J Alloys Compd 662:421–430. https://doi.org/10.1016/j.jallcom.2015.12.062

Zhou G, Wang Y, Zhou R, Wang C, Jin Y, Qiu J et al (2019) Synthesis of amino-functionalized bentonite/$CoFe_2O_4$@MnO_2 magnetic recoverable nanoparticles for aqueous Cd^{2+} removal. The Sci Total Environ 682:505–513. https://doi.org/10.1016/j.scitotenv.2019.05.218